Science
AAAS

Evidence for Obliquity Forcing of Glacial Termination II

R. N. Drysdale, *et al.*

Science **325**, 1527 (2009);
DOI: 10.1126/science.1170371

Science (print ISSN 0036-8075; online ISSN 1095-9203) is published weekly, except the last week in December, by the American Association for the Advancement of Science, 1200 New York Avenue NW, Washington, DC 20005.

occur only if orbital maturity has been achieved (*19*, *20*). The fact that BR was on a mature Aten orbit supports this suggestion. We explored BR's most recent orbital history, finding approaches as close as 0.04 AU (distance to within a factor of 2) for an encounter with Venus in September 2001, and earlier close approaches with Earth [a search for BR precursor objects in NEO space was also made (*5*)]. In addition, we used a numerical method designed to model the evolution of NEO orbits (*21*) to determine the probability that BR came from a specific NEO source region, given its present-day semimajor axis, eccentricity, and inclination (this approach is based on the assumption that small NEOs have the same orbital distribution as observed kilometer-sized NEOs). The probability of BR coming from the innermost region of the main belt is 98%. There is a 72% probability that it was delivered from the ν_6 resonance, a 26% probability that it came from one of the numerous small resonances in the inner main belt, and a 2% probability that it came from the 3:1 resonance. The outer main belt (>2.8 AU) and the Jupiter-family comet population can be ruled out as possible sources.

The BR parent body would likely be classified as a V-type asteroid. The characteristics of a reflectance spectrum are largely controlled by the major-element chemistry of the dominant phases, principally pyroxene (*7*). Because the major-element composition of BR's pyroxene (and plagioclase) (fig. S2) (*16*), modal mineral abundance (*17*), and grain size (fig. S1) are similar to those of normal eucrites, the reflectance spectrum should also be very similar to that of normal eucrites (i.e., it should match that of V-type asteroids). There are few V-type asteroids that are dynamically distinct from 4 Vesta (*22*, *23*). In the inner main belt, most V-types are part of the Vesta dynamical family [the proximity of a few V-types to resonances was a fundamental link in the conceptual chain connecting 4 Vesta with HED meteorites (*3*)]. Even for those inner main belt V-types that are not currently part of the Vesta dynamical family, it is difficult to exclude an origin at Vesta (*24*–*26*). In the case of BR, compositional as well as orbital data indicate that basaltic asteroids unrelated to 4 Vesta reside in the innermost main belt, and that these bodies are delivering material (most likely via the ν_6 resonance) into Earth-crossing orbits.

Finally, the predicted source region of BR is consistent with a recent planetesimal evolution model (*27*). In this model, planetesimals forming in the terrestrial planet region, which would have had fast accretion times relative to main belt objects, would also have been more likely to melt (from decay of short-lived radionuclides such as ^{26}Al) than later-accreting chondrites. The collisional evolution of these planetesimals would result in fragments, some of which (according to numerical simulations) would have been scattered into the main belt via interactions with planetary embryos (*27*). The model provides an explanation both for the paucity of differentiated asteroids in the main belt and for the anomalously old ages for differentiated meteorites [e.g., (*28*)]. The greatest concentration of surviving fragments should be in the innermost main belt (*27*), the most probable starting location for the BR precursor.

References and Notes

1. P. Spurný, J. Oberst, D. Heinlein, *Nature* **423**, 151 (2003).
2. P. Jenniskens *et al.*, *Nature* **458**, 485 (2009).
3. Meteoritical Bulletin Database (http://tin.er.usgs.gov/meteor/metbull.php).
4. A. W. R. Bevan, R. A. Binns, *Meteoritics* **24**, 127 (1989).
5. See supporting material on *Science* Online.
6. R. P. Binzel, S. Xu, *Science* **260**, 186 (1993).
7. T. H. Burbine *et al.*, *Meteorit. Planet. Sci.* **36**, 761 (2001).
8. A. Yamaguchi *et al.*, *Science* **296**, 334 (2002).
9. Oxygen isotopic analyses are reported in standard δ notation where δ18O has been calculated as: $\delta^{18}O = [\{(^{18}O/^{16}O)_{sample}/(^{18}O/^{16}O)_{ref}\} - 1] \times 1000$ per mil (‰), and similarly for $\delta^{17}O$ using the $^{17}O/^{18}O$ ratio. The reference standard is Vienna Standard Mean Ocean Water (VSMOW). $\Delta^{17}O$, which represents the deviation from the terrestrial fractionation line, has been calculated using the linearized format of Miller (2002): $\Delta^{17}O = 1000\ln(1 + (\delta^{17}O/1000)) - \lambda 1000\ln(1 + (\delta^{18}O/1000))$ where $\lambda = 0.5247$ (*29*).
10. R. C. Greenwood, I. A. Franchi, A. Jambon, P. C. Buchanan, *Nature* **435**, 916 (2005).
11. E. R. D. Scott, R. C. Greenwood, I. A. Franchi, I. S. Sanders, *Geochim. Cosmochim. Acta* 10.1016/j.gca.2009.06.024 (2009).
12. E. R. D. Scott *et al.*, *Lunar Planet. Sci. Conf.* **XXXIX**, abstr. 2344 (2008).
13. U. H. Wiechert, A. N. Halliday, H. Palme, D. Rumble, *Earth Planet. Sci. Lett.* **221**, 373 (2004).
14. D. W. Mittlefehldt, *Meteorit. Planet. Sci.* **40**, 665 (2005).
15. R. Lentz, E. R. D. Scott, T. J. McCoy, *Lunar Planet. Sci. Conf.* **XXXVIII**, abstr. 1968 (2007).
16. Based only on mineralogy and mineral chemistry considerations, BR would be classified as a basaltic eucrite. Original pyroxene is an Fe-rich pigeonite with augite exsolution lamellae, and Fe/Mn ratio of 31.5 ± 1.3, within the range for normal eucrites. Plagioclase major ($An_{84.1–94.9}$) and minor (K_2O = 0.03 to 0.09 wt%) compositions lie within the ranges reported for basaltic eucrites, as do chromite compositions (Al_2O_3 = ~7 wt%; TiO_2 = ~3.5 wt%).
17. Modal mineralogy from x-ray diffraction position sensitive detector analysis (*5*): silica = 4.5 vol%, plagioclase = 52.5 vol%, pyroxene = 41.5 vol%, minor opaques = 1.5 vol%.
18. A. J. G. Jurewicz, D. W. Mittlefehldt, J. H. Jones, *Geochim. Cosmochim. Acta* **57**, 2123 (1993).
19. R. Greenberg, M. C. Nolan, in *Asteroids II*, R. P. Binzel, T. Gehrels, M. S. Matthews, Eds. (Univ. of Arizona Press, Tucson, AZ, 1989), pp. 778–804.
20. Orbital maturity is the tendency for NEOs to evolve to more Earth-like orbits, and then Aten-like orbits, from orbital paths that initially took them out to the asteroid belt.
21. W. F. Bottke *et al.*, *Icarus* **156**, 399 (2002).
22. D. Lazzaro *et al.*, *Science* **288**, 2033 (2000).
23. N. A. Moskovitz *et al.*, *Icarus* **198**, 77 (2008).
24. V. Carruba *et al.*, *Icarus* **162**, 308 (2003).
25. V. Carruba *et al.*, *Astron. Astrophys.* **441**, 819 (2005).
26. D. Nesvorný *et al.*, *Icarus* **193**, 85 (2008).
27. W. F. Bottke Jr. *et al.*, *Nature* **439**, 821 (2006).
28. T. Kleine *et al.*, *Geochim. Cosmochim. Acta* **69**, 5805 (2005).
29. M. F. Miller, *Geochim. Cosmochim. Acta* **66**, 1881 (2002).

30. Supported by UK Science and Technology Facilities Council grants PP/C502406/1 and ST/F003072/1; grant 205/08/0411 of the Czech Science Foundation; and EU grant MRTN-CT-2006-035519. P.S. thanks the Czech Academy of Sciences for support through institutional research project AV0Z10030501. We also thank the people of the Nullarbor, and M. Cupák, M. Halík, J. Ullrich, A. Forte, M. Creasy, L. Beazley, T. Smith, C. Daw, T. Kennedy, G. Kennedy, W. Moore, T. Davies, and the trustees of the Western Australian Museum for their help and support over the course of this project, and Australia Post for in-kind sponsorship.

Supporting Online Material

www.sciencemag.org/cgi/content/full/325/5947/1525/DC1
Materials and Methods
Figs. S1 and S2
Table S1
References

9 April 2009; accepted 24 July 2009
10.1126/science.1174787

Evidence for Obliquity Forcing of Glacial Termination II

R. N. Drysdale,[1]* J. C. Hellstrom,[2] G. Zanchetta,[3,4,5] A. E. Fallick,[6] M. F. Sánchez Goñi,[7] I. Couchoud,[1] J. McDonald,[1] R. Maas,[2] G. Lohmann,[8] I. Isola[4]

Variations in the intensity of high-latitude Northern Hemisphere summer insolation, driven largely by precession of the equinoxes, are widely thought to control the timing of Late Pleistocene glacial terminations. However, recently it has been suggested that changes in Earth's obliquity may be a more important mechanism. We present a new speleothem-based North Atlantic marine chronology that shows that the penultimate glacial termination (Termination II) commenced 141,000 ± 2500 years before the present, too early to be explained by Northern Hemisphere summer insolation but consistent with changes in Earth's obliquity. Our record reveals that Terminations I and II are separated by three obliquity cycles and that they started at near-identical obliquity phases.

During the Late Pleistocene, the period of glacial-to-interglacial transitions (or terminations) has increased relative to the Early Pleistocene [~100 thousand years (ky) versus 40 ky] (*1*, *2*). A coherent explanation for this shift still eludes paleoclimatologists (*3*). Although many different models have been proposed (*4*), the most widely accepted one invokes changes in the intensity of high-latitude Northern Hemisphere summer insolation (NHSI). These changes are driven largely by the precession of the equinoxes (*5*), which produces relatively large

seasonal and hemispheric insolation intensity anomalies as the month of perihelion shifts through its ~23-ky cycle.

Recently, a convincing case has been made for obliquity control of Late Pleistocene terminations (*4*), which is a feasible hypothesis because of the relatively large and persistent increases in total summer energy reaching the high latitudes of both hemispheres during times of maximum Earth tilt. Indeed, the obliquity period has been found to be an important spectral component in methane (CH_4) and paleotemperature records from Antarctic ice cores (*6*, *7*).

Testing the obliquity and other orbital-forcing models requires precise chronologies through terminations, which are best recorded by oxygen isotope ratios of benthic foraminifera ($\delta^{18}O_b$) in deep-sea sediments (*1*, *8*). Although affected by deep-water temperature (T_{dw}) and composition ($\delta^{18}O_{dw}$) variations triggered by changes in circulation patterns (*9*), $\delta^{18}O_b$ signatures remain the most robust measure of global ice-volume changes through terminations. Unfortunately, dating of marine sediment records beyond the limits of radiocarbon methods has long proved difficult, and only Termination I [T-I, ~18 to 9 thousand years ago (ka)] has a reliable independent chronology. Most marine chronologies for earlier terminations rely on the SPECMAP orbital template (*8*) with its a priori assumptions of insolation forcing and built-in phase lags between orbital trigger and ice-sheet response. Although SPECMAP and other orbital-based age models serve many important purposes in paleoceanography, their ability to test climate-forcing hypotheses is limited because they are not independent of the hypotheses being tested. Consequently, the inability to accurately date the benthic record of earlier terminations constitutes perhaps the single greatest obstacle to unraveling the problem of Late Pleistocene glaciations.

Of the pre–T-I Late Pleistocene terminations, Termination II (T-II) has generated greatest interest. Several previous attempts to establish its timing from radiometrically dated archives have challenged the NHSI model (*10*–*12*). Arguably, the best known is the Devils Hole (DH) vein calcite record (*10*), which placed the timing of T-II ~15 ky earlier than that of the SPECMAP model prediction. Although now considered to be a regional rather than a global paleoclimate proxy (*13*), it highlighted the potential of using radiometrically datable archives to test climate-forcing hypotheses. Since then, radiometric ages on corals and detrital marine carbonates have been used to constrain sea levels during and immediately after T-II (*11*, *12*, *14*). However, this approach has proved controversial because of open-system effects on marine carbonate ages (*15*), which are difficult to deconvolve and correct (*16*).

To determine the age of T-II, we applied the uranium-thorium (U-Th) chronology from a high-resolution speleothem $\delta^{18}O$ time series to the T-II marine sediment record from the Iberian margin (*9*, *17*–*21*) in the northeast North Atlantic Ocean (fig. S1). The North Atlantic is highly sensitive to terminations because of its role in the global conveyor belt of oceanic circulation and its proximity to Northern Hemisphere ice sheets (*9*). The Iberian margin sediments preserve an excellent multi-proxy paleoclimate record through T-II and the Last Interglacial (*9*, *17*–*21*) (figs. S10 and S11). Our speleothem time series was assembled by using three stalagmites from Antro del Corchia, an Italian cave system that receives most of its recharge rainfall via westerly air masses crossing the North Atlantic (*22*). The stalagmite time series extends between ~120 and ~146 ka (Fig. 1) and is based on over 1400 oxygen isotope measurements fixed in absolute time by 56 mass spectrometric U-Th ages (tables S1 and S2 and figs. S3, S8, and S9).

The correspondence between Corchia $\delta^{18}O$ and Iberian-margin sea-surface temperatures (SSTs) through T-II (Fig. 2) is remarkable. Although the mechanisms that force speleothem $\delta^{18}O$ varia-

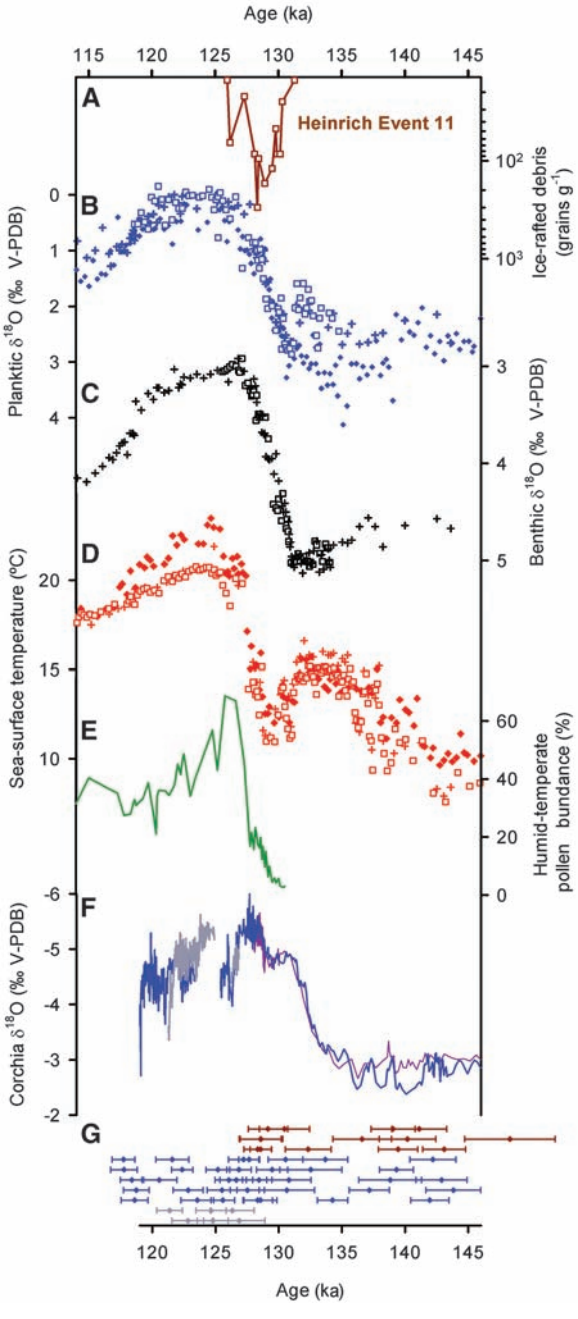

Fig. 1. Iberian-margin data from cores MD95-2042 [(*20*, *21*) crosses], MD01-2444 [(*9*, *18*) open squares], and ODP-977A [(*17*, *18*) solid diamonds] placed on the ODP-977A time scale of (*18*) and the stacked Corchia speleothem $\delta^{18}O$ data. (**A**) Ice-rafted debris from MD01-2444 (*9*) (plotted on an inverted logarithmic scale). (**B**) Planktic foraminifera $\delta^{18}O$ (*Globigerina bulloides*) from MD95-2042 (*20*), MD01-2444 (*9*), and ODP-977A (*17*). (**C**) Benthic foraminifera $\delta^{18}O$ from MD95-2042 (*20*) (mixed species) and MD01-2444 (*9*) (*Globobulimina affinis*). (**D**) $U^{k'}_{37}$ alkenone-based SSTs from ODP-977A (*17*), MD01-2444 (*18*), and MD95-2042 (*21*). (**E**) Percentage abundance of warm humid-temperate pollen (Eurosiberian plus Mediterranean taxa) from MD95-2042 (*20*). (**F**) Corchia speleothem $\delta^{18}O$ profiles from stalagmites CC5 (blue), CC1 (maroon), and CC7 (gray). (**G**) Corchia speleothem radiometric ages with 95% error bars [same color scheme as in (F)].

[1]Environmental and Climate Change Group, University of Newcastle, Callaghan, New South Wales 2308, Australia. [2]School of Earth Sciences, University of Melbourne, Parkville, Victoria 2010, Australia. [3]Department of Earth Sciences, University of Pisa, Pisa 56100, Italy. [4]Istituto Nazionale di Geofisica e Vulcanologia, via della Fagiola, Pisa 56126, Italy. [5]IGG-CNR, Via Moruzzi, 1 56100 Pisa, Italy. [6]Scottish Universities Environmental Research Centre, East Kilbride G75 0GF, UK. [7]EPHE, UMR CNRS 5805 EPOC, Université Bordeaux 1, 33405 Talence, France. [8]Alfred Wegener Institute for Polar and Marine Research, Bussestrasse 24, D-27570 Bremerhaven, Germany.

*To whom correspondence should be addressed. E-mail: russell.drysdale@newcastle.edu.au

tions are complex (*23*), we believe that Corchia $\delta^{18}O$ is driven largely by variations in rainfall amount (*22*, *24*) in response to changes in regional SSTs. Previous studies from Corchia show that speleothem $\delta^{18}O$ is sensitive to past changes in North Atlantic circulation at both orbital (*22*, *25*) and millennial time scales (*26*), with $\delta^{18}O$ increasing during colder (glacial or stadial) phases and the reverse occurring during warmer (interglacial or interstadial) phases. During glacial/stadial periods, weaker North Atlantic meridional overturning circulation (MOC) results in a southward shift in the polar front (*20*), bringing cooler ocean waters into the middle latitudes, including the western Mediterranean Sea (*27*). The decline in regional air temperatures, evaporation, and moisture transport toward the Italian peninsula would lower the amount of rainfall reaching Corchia Cave, producing elevated stalagmite $\delta^{18}O$ values because of a reduction in the rainfall "amount effect" (*24*), a phenomenon well recognized in other Mediterranean speleothem records (*28*, *29*). Under warm conditions, more intensive MOC increases regional SSTs and displaces the polar front retreats to higher latitudes. This favors increased air temperatures, evaporation, and moisture advection across the Mediterranean, generating higher rainfalls in the Corchia region and lower speleothem $\delta^{18}O$ values. Stronger MOC may contribute more isotopically depleted North Atlantic–sourced vapor compared with western Mediterranean–sourced vapor (*30*), further depressing the isotopic values during warm intervals. Although factors such as changes in surface ocean composition, cave and regional air temperatures, and the seasonality of rainfall would affect speleothem $\delta^{18}O$ signatures through a termination (*23*), independent support for the forcing of Corchia $\delta^{18}O$ predominantly by rainfall amount is provided by trace element, initial uranium isotope ratio, and growth rate changes in these speleothems (figs. S4 to S7).

To investigate the Iberian marine sequence through T-II in more detail, we produced a multiproxy "Iberian-margin stack" on a common time scale by tuning the MD01-2444 (*9*, *18*) and MD95-2042 (*19*–*21*) data to the ODP-977A chronology (*17*, *18*) with use of the benthic and SST profiles (figs. S10 and S11). We then tuned the ODP-977A SST series to the precisely dated Corchia $\delta^{18}O$ series (Fig. 2A), enabling us to transfer the multiproxy Iberian-margin stack onto the Corchia radiometric time scale (Fig. 2, B to F, and fig. S12). The radiometrically tuned marine sequence through T-II shows that the monotonic decrease in $\delta^{18}O_b$ from cores MD01-2444 and MD95-2042 starts at 141 ± 2.5 ka (black arrow, Fig. 2C), heralding the commencement of the termination. It was demonstrated recently (*9*) that $\delta^{18}O_b$ from the Iberian margin during T-I and T-II were affected by changes in T_{dw} and $\delta^{18}O_{dw}$ because of variations in MOC and North Atlantic Deep Water (NADW) formation, thus corrupting the otherwise predominant ice-volume signature of $\delta^{18}O_b$. However, at the time of the initial $\delta^{18}O_b$ decrease these variations are negligible (Fig. 2D), indicating that $\delta^{18}O_b$ faithfully records the onset of deglaciation. Lastly, we constrain the timing of ice-rafted debris flux reaching the Iberian margin [and associated with Heinrich Event 11 (H11) (*31*)] to between 140 ± 2.5 and 129 ± 1.5 ka (Fig. 2B).

SSTs experienced their first steady increase at 136 ± 2.5 ka (Fig. 2A), that is, at about the T-II midpoint. Together with the abrupt decrease in $\delta^{18}O_{dw}$ and increase in T_{dw} (Fig. 2D), this suggests a resumption of NADW formation at this time in response to a stronger MOC (*14*). The clear interruption to the monotonic decrease in Iberian $\delta^{18}O_b$ values between 136 and 134 ka (blue arrow, Fig. 2C) occurs about two-thirds of the way through the deglacial benthic shift, suggesting relatively high sea levels by this time. Concurrent increases in T_{dw}, $\delta^{18}O_{dw}$, and SSTs support intensified MOC (*14*), which runs counter to previous suggestions of substantially renewed ice-sheet growth and sea-level fall (*32*). The rise in SSTs is interrupted twice by pauses (~135 to 132.5 ka and ~131.5 to 129.5 ka), both of which are expressed in the Corchia $\delta^{18}O$ record (Fig. 2A). The oldest probably coincides with the post-Zeifen stadial (*20*), whereas the latter occurs just after the sharp rise in humid-temperate Eurosiberian and Mediterranean taxa that marks the start of the Eemian vegetation phase in southern Europe (*20*) (Fig. 2F). The close association between the abrupt SST rise off Iberia and increasing forest cover between these two pauses (~132.5 to 131.5 ka) is consistent with a recent age estimate of the abrupt postglacial increase in global CH_4 (131.2 ± 2 ka) (*14*).

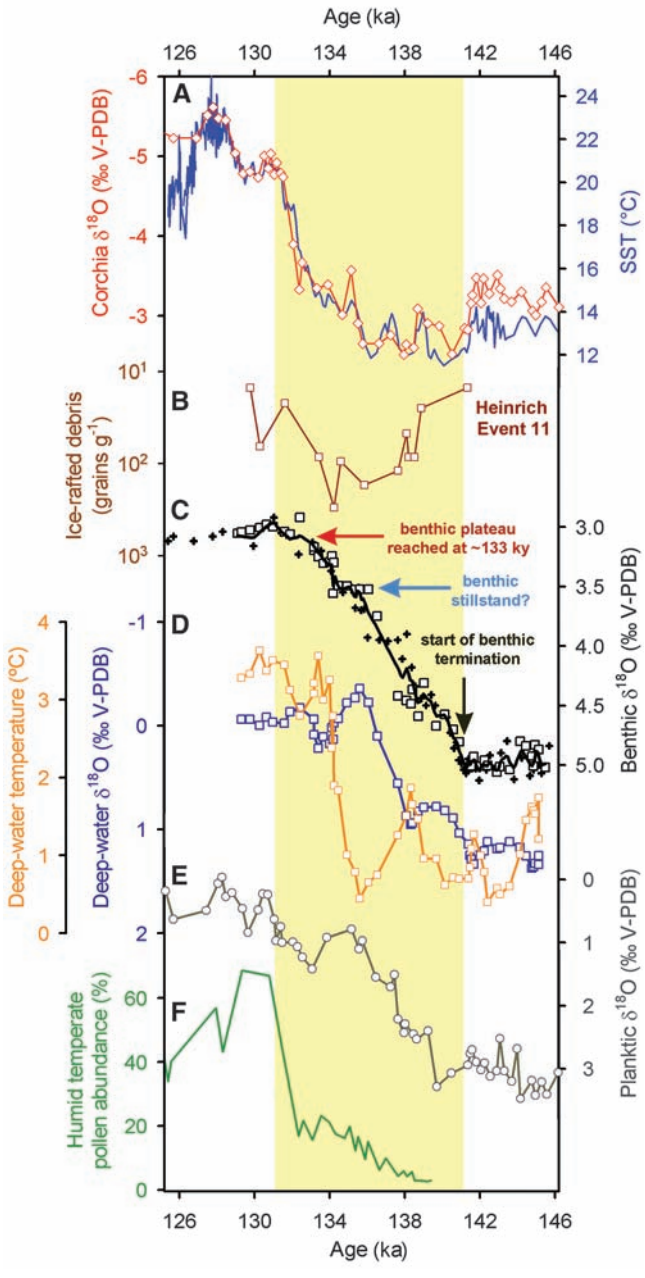

Fig. 2. The Iberian-margin sequence from Fig. 1 replotted on the Corchia radiometric time scale by matching the $\delta^{18}O$ from stalagmite CC5 to the ODP-977A SST (*23*). (**A**) Overlay of Corchia $\delta^{18}O$ and ODP-977A SST (*17*) showing the close structural correspondence between the two records. The greater sampling resolution accounts in part for the higher variability in the stalagmite $\delta^{18}O$. (**B**) Ice-rafted debris (grains g^{-1}) from Heinrich Event 11 from MD01-2444 (*9*) (plotted on an inverted, logarithimic scale). (**C**) Benthic foraminifera $\delta^{18}O$ from MD01-2444 [open squares (*9*)] and MD95-02042 [crosses (*20*)]. (**D**) Deep-water temperature changes based on Mg/Ca ratios of benthic foraminifera (orange squares) and deep-water $\delta^{18}O$ variations (dark blue squares) through T-II from MD01-2444 [three-point smoothing, replotted from original data in (*9*)]. (**E**) Planktic foraminifera $\delta^{18}O$ from ODP-977A (*17*). (**F**) Percentage abundance of warm humid-temperate pollen (Eurosiberian and Mediterranean taxa) from MD95-2042 (*20*). The yellow section is the approximate period of T-II on the basis of the benthic $\delta^{18}O$.

Our results can be used to explore the phase relationships between sea level, $\delta^{18}O_b$, and the Last Interglacial SST optimum (*14*). During T-I, the "benthic plateau" (*33*) was attained by 10.1 ± 0.5 ka (*34*), when sea levels were ~40 m below present (40 mbsl) (*35*), and preceded the Holocene SST maximum off the Iberian margin (8 to 9 ka) by about 1 to 2 ky (*17*, *18*) and the Holocene highstand (6.4 ± 1 ka) by 3.7 ± 1.1 ky (*14*). After T-II, SSTs off Iberia peaked between ~129 ± 1.5 and ~127 ± 2 ka (Fig. 2A) according to our record, ~4 ky after the start of our benthic plateau (~133 ± 2 ka; red arrow in Fig. 2C). This gives a SST–benthic plateau lag longer than that for T-I. As for the timing of the Last Interglacial sea-level highstand, age estimates based on coral U-series dating vary widely depending on whether open- or closed-system assumptions are used (*15*, *36*). Such estimates must be regarded as minima given likely preservation biases resulting from erosion (*16*). The oldest reported closed-system age constraint from a tectonically stable margin placed the highstand onset at ~129 ± 1 ka (*36*), yielding a benthic plateau–sea-level highstand lag almost identical to that of T-I (*14*), whereas a highstand age of 126 ± 1.7 ka has been determined from open-system–corrected coral ages (*14*, *15*). A recent sea-level reconstruction for T-II (*37*) suggested a sea level of 30 mbsl at the time when the benthic plateau is reached, similar to that for T-I (40 mbsl) (*14*, *35*). This reconstruction, which has been chronologically anchored in part by ~137-ky-old corals that define a minimum age estimate for sea level at 85 mbsl, suggests a T-II starting point at ~141 ka (*37*). This is in excellent agreement with our revised benthic curve (Fig. 2C).

Our radiometric age–based benthic sequence provides a new opportunity to investigate orbital forcing and the timing of the last two glacial terminations. We compared the benthic record from MD95-2042 for T-I and T-II with changes in the intensity of high-latitude Northern and Southern Hemisphere summer insolation and Earth's obliquity (Fig. 3). We find that NHSI intensity is unlikely to be the driving force for T-II: Intensity values are close to minimum at the time of the start of T-II, and a lagged response to the previous insolation peak at ~148 ka is unlikely because of its low amplitude (Fig. 3A). This argues against the SPECMAP curve being a reliable age template through T-II, given the age offset of ~8 ky for the T-II midpoint (*8*) with respect to our record. A much stronger case can be made for obliquity as a forcing mechanism. On the basis of our results (Fig. 3B), both T-I and T-II commence at the same phase of obliquity, and the period between them is exactly equivalent to three obliquity cycles (~123 ky). Obliquity is clearly very important during the Early Pleistocene (*2*, *38*), and recently (*4*, *39*) a compelling argument was advanced that Late Pleistocene terminations are also forced by obliquity but that they bridge multiple obliquity cycles. Under this model, predominantly obliquity-driven total summer energy is considered more important in forcing terminations than the classical precession-based peak summer insolation model, primarily because the length of summer decreases as the Earth moves closer to the Sun. Hence, increased insolation intensity resulting from precession is offset by the shorter summer duration, with virtually no net effect on total summer energy in the high latitudes (*4*, *39*). By contrast, larger angles of Earth tilt lead to more positive degree days in both hemispheres at high latitudes, which can have a more profound effect on the total summer energy received and can act essentially independently from a given precession phase (*4*, *39*). The effect of obliquity on total summer energy is more persistent at large tilt angles, lasting up to 10 ky (*39*), because of the relatively long period of obliquity. Lastly, in a given year the influence of maximum obliquity persists for the whole summer, whereas at maximum precession early summer positive insolation anomalies are cancelled out by late summer negative anomalies, limiting the effect of precession over the whole summer (*39*).

Although the precise three-cycle offset between T-I and T-II in our radiometric chronology and the phase relationships shown in Fig. 3 together argue strongly for obliquity forcing, the question remains whether obliquity changes alone are responsible. Recent work (*40*) invoked an "insolation-canon," whereby terminations are Southern Hemisphere–led but only triggered at times when insolation in both hemispheres is increasing simultaneously, with SHSI approaching maximum and NHSI just beyond a minimum. However, it is not clear that relatively low values of NHSI (at times of high SHSI) should play a role in deglaciation. An alternative is an insolation canon involving SHSI and obliquity. For T-I and T-II, the benthic $\delta^{18}O$ decrease commences when SHSI and obliquity reach similar values, with SHSI leading obliquity in both cases. During the two intervening obliquity cycles, SHSI lags obliquity. Thus, relatively high SHSI may instigate initial warming in the south. This may continue as the system approaches maximum obliquity, after which sustained and higher total summer energy occurs. The notion of Southern Hemisphere–led terminations is nothing new (*41*), but the mechanism or mechanisms that sustain this warming to the point where a termination is triggered have not previously been elucidated. A canon involving a lagging obliquity may well be the answer. Assembling similar records for earlier terminations will further test this model. Our study demonstrates

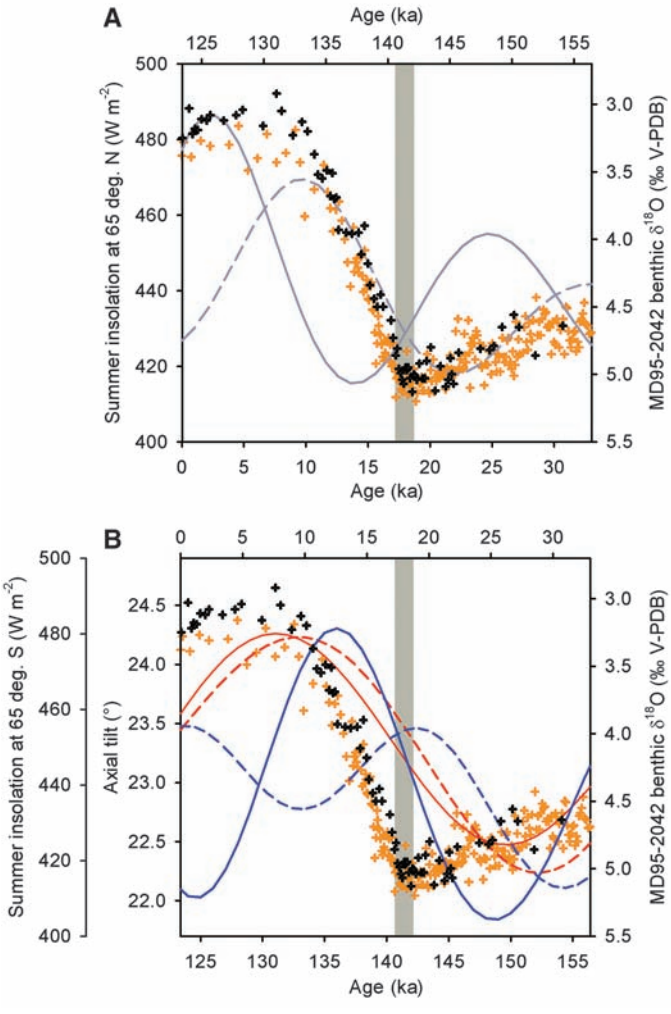

Fig. 3. Comparison between the benthic $\delta^{18}O$ record through T-I [orange crosses; plotted on the time scale of (*21*)] and T-II (black crosses; replotted on the Corchia time scale, this study) from core MD95-2042, showing similarity in the duration of both terminations and orbital parameters. (**A**) NHSI at 65°N (gray) for T-I (dashed line) and T-II (solid line). (**B**) SHSI at 65°S (blue) and obliquity curves (red) for T-I (dashed lines) and T-II (solid lines) and obliquity. The gray vertical bars linking the age axes mark the commencement points for both terminations and reveal that the age difference is equivalent to three obliquity cycles (~123 ky).

that precisely dated speleothems can play a key role in constraining the timing of earlier terminations, provided that close coupling with marine paleoclimate records can be demonstrated.

References and Notes

1. N. J. Shackleton, N. D. Opdyke, *Quat. Res.* **3**, 39 (1973).
2. M. E. Raymo, K. Nisancioglu, *Paleoceanography* **18**, 1011 (2003).
3. M. E. Raymo, P. Huybers, *Nature* **451**, 284 (2008).
4. P. Huybers, C. Wunsch, *Nature* **434**, 491 (2005).
5. M. Milankovitch, *Kanon der Erdbestrahlung und seine Kanon der Erdbestrahlung und seine Andwendung auf das Eiszeitenproblem* (Royal Serbian Academy, Belgrade, 1941).
6. J. Jouzel *et al.*, *Science* **317**, 793 (2007); published online 3 July 2007 (10.1126/science.1141038).
7. L. Loulergue *et al.*, *Nature* **453**, 383 (2008).
8. D. G. Martinson *et al.*, *Quat. Res.* **27**, 1 (1987).
9. L. C. Skinner, N. J. Shackleton, *Quat. Sci. Rev.* **25**, 3312 (2006).
10. I. J. Winograd *et al.*, *Science* **258**, 255 (1992).
11. G. M. Henderson, N. C. Slowey, *Nature* **404**, 61 (2000).
12. C. D. Gallup, H. Cheng, F. W. Taylor, R. L. Edwards, *Science* **295**, 310 (2002).
13. T. D. Herbert *et al.*, *Science* **293**, 71 (2001); published online 7 June 2001 (10.1126/science.1059209).
14. C. Waelbroeck *et al.*, *Earth Planet. Sci. Lett.* **265**, 183 (2008).
15. W. G. Thompson, S. L. Goldstein, *Science* **308**, 401 (2005).
16. G. M. Henderson, L. F. Robinson, K. Cox, A. L. Thomas, *Quat. Sci. Rev.* **25**, 3346 (2006).
17. B. Martrat *et al.*, *Science* **306**, 1762 (2004).
18. B. Martrat *et al.*, *Science* **317**, 502 (2007); published online 14 June 2007 (10.1126/science.1139994).
19. M. F. Sánchez Goñi *et al.*, *Earth Planet. Sci. Lett.* **231**, 111 (2005).
20. M. F. Sánchez Goñi, F. Eynaud, J. L. Turon, N. J. Shackleton, *Earth Planet. Sci. Lett.* **171**, 123 (1999).
21. D. Pailler, E. Bard, *Palaeogeogr. Palaeoclimatol. Palaeoecol.* **181**, 431 (2002).
22. R. N. Drysdale *et al.*, *Earth Planet. Sci. Lett.* **227**, 215 (2004).
23. Materials and methods are available as supporting material on *Science* Online.
24. W. Dansgaard, *Tellus* **16**, 436 (1964).
25. R. N. Drysdale, G. Zanchetta, J. C. Hellstrom, A. E. Fallick, J. X. Zhao, *Geophys. Res. Lett.* **32**, L24708 (2005).
26. R. N. Drysdale *et al.*, *Geology* **35**, 77 (2007).
27. I. Cacho *et al.*, *Paleoceanography* **14**, 698 (1999).
28. E. Bard, F. Antonioli, S. Silenzi, *Earth Planet. Sci. Lett.* **196**, 135 (2002).
29. M. Bar-Matthews, A. Ayalon, M. Gilmour, A. Matthews, C. Hawkesworth, *Geochim. Cosmochim. Acta* **67**, 3181 (2003).
30. H. Celle-Jeanton, Y. Travi, B. Blavoux, *Geophys. Res. Lett.* **28**, 1215 (2001).
31. H. Heinrich, *Quat. Res.* **29**, 142 (1988).
32. T. M. Esat, M. T. McCulloch, J. Chappell, B. Pillans, A. Omura, *Science* **283**, 197 (1999).
33. N. J. Shackleton, M. Chapman, M. F. Sánchez Goñi, D. Pailler, Y. Lancelot, *Quat. Res.* **58**, 14 (2002).
34. M. Siddall, E. Bard, E. J. Rohling, C. Hemleben, *Geology* **34**, 817 (2006).
35. M. Siddall *et al.*, *Nature* **423**, 853 (2003).
36. C. H. Stirling, T. M. Esat, K. Lambeck, M. T. McCulloch, *Earth Planet. Sci. Lett.* **160**, 745 (1998).
37. A. L. Thomas *et al.*, *Science* **324**, 1186 (2009); published online 23 April 2009 (10.1126/science.1168754).
38. P. Huybers, *Science* **313**, 508 (2006); published online 21 June 2006 (10.1126/science.1125249).
39. P. Huybers, *Quat. Sci. Rev.* **26**, 37 (2007).
40. K. G. Schulz, R. E. Zeebe, *Earth Planet. Sci. Lett.* **249**, 326 (2006).
41. G. Knorr, G. Lohmann, *Nature* **424**, 532 (2003).

42. We acknowledge the comments of P. Huybers, S. Frisia, R. Lever, P. Hoare, and three anonymous reviewers and thank A. Berger, B. Martrat, and L. Skinner for providing data. Laboratory and drafting assistance was provided by T. Smith, S. Komar, A. Tait, J. Dougans, and O. Rey-Lescure. This research was funded by the Federazione Speleologica Toscana, the University of Newcastle, and the Australian Research Council (DP0773700) and falls within the framework of the Scottish Alliance for Geoscience, Environment, and Society (SAGES).

Supporting Online Material

www.sciencemag.org/cgi/content/full/1170371/DC1
Materials and Methods
Figs. S1 to S15
Tables S1 and S2
References

30 December 2008; accepted 22 July 2009
Published online 13 August 2009;
10.1126/science.1170371
Include this information when citing this paper.

Cellular Basis of Itch Sensation

Yan-Gang Sun,[1]* Zhong-Qiu Zhao,[1]* Xiu-Li Meng,[1,2] Jun Yin,[1] Xian-Yu Liu,[1] Zhou-Feng Chen[1]†

Itch and pain are two distinct sensations. Although our previous study suggested that gastrin-releasing peptide receptor (GRPR) is an itch-specific gene in the spinal cord, a long-standing question of whether there are separate neuronal pathways for itch and pain remains unsettled. We selectively ablated lamina I neurons expressing GRPR in the spinal cord of mice. These mice showed profound scratching deficits in response to all of the itching (pruritogenic) stimuli tested, irrespective of their histamine dependence. In contrast, pain behaviors were unaffected. Our data also suggest that GRPR$^+$ neurons are different from the spinothalamic tract neurons that have been the focus of the debate. Together, the present study suggests that GRPR$^+$ neurons constitute a long-sought labeled line for itch sensation in the spinal cord.

Itch has long been considered to be a submodality or subquality of pain (*1*–*4*), because the two sensations share many similarities (*5*). Whether itch and pain, two distinct sensations, are mediated by distinct neural circuits has been the subject of controversy (*6*–*8*). In the spinal cord, arguments for the "labeled line" came from electrophysiological recordings in cat showing the presence of a small subset of histamine-responsive, mechanically, thermally and mustard oil insensitive lamina I spinothalamic tract (STT) neurons (*9*). Recent studies in primates, however, found that all histamine-sensitive STT neurons were responsive to noxious mechanical and chemical stimuli, notably capsaicin, arguing against the "labeled line" for itch (*10*, *11*). Although our previous data suggested that gastrin-releasing peptide receptor (GRPR) is an itch-specific gene in the spinal cord (*12*), they could not be extrapolated to imply that GRPR$^+$ neurons are itch specific, simply because neurons expressing one sensory modality–specific gene may also express other sensory modality–specific genes, as often seen in sensory neurons (*13*). One way to address this issue is to selectively ablate a subset of itch-signaling neurons and assess whether pain behaviors are altered in the absence of these neurons. We selectively ablated GRPR$^+$ neurons in the spinal cord of mice by intrathecal administration of bombesin-saporin (bombesin-sap), a toxin coupled to bombesin that binds with high affinity to GRPR and results in GRPR internalization along with bombesin-sap and cell death (fig. S1) (*14*, *15*).

We first determined the optimal dose and time course of bombesin-sap treatment. Intrathecal injection of bombesin-sap ablated GRPR$^+$ neurons and reduced pruritogen-induced scratching behaviors in a dose-dependent manner (fig. S2). Most of GRPR$^+$ neurons (>75%) were lost 2 weeks after single intrathecal injection of bombesin-sap (400 ng) (Fig. 1, A to C). To determine the specificity of bombesin-sap treatment, we analyzed several subpopulations of neurons in the spinal cord by using lamina-specific molecular markers. Expression of neuromedin U receptor 2 (NMUR2) and prodynorphin was not affected in lamina I of mice treated with bombesin-sap (Fig. 1, D to F, and fig. S3), nor was neurokinin 1 receptor (NK1) (Fig. 1, G to I), a lamina I and III gene expressed in a subset of neurons known for their involvement in nociceptive transmission (*15*, *16*). Expression of lamina II markers such as neurotensin and PKCγ in the bombesin-sap group was also not affected (Fig. 1, J to O), nor was the projection of primary afferents (fig. S4). Saporin conjugated to a random peptide sequence (blank-sap) did not show cytotoxicity effects (figs. S4 and S5).

We next examined scratching behaviors of mice treated with bombesin-sap in response to intradermal injection of a panel of histamine-dependent pruritogenic agents. Unlike the control mice, which exhibited vigorous scratching response after intradermal injection of histamine, bombesin-sap–treated mice showed profound scratching deficits (reduced by 77%) (Fig. 2A). Scratching behaviors evoked by compound 48/80 (*17*) and serotonin [5-hydroxytryptamine (5-HT)] were also dramatically reduced relative to the control mice (by 79% and 88%, respectively) (Fig. 2, B and C, and fig. S9D). We further examined scratching behavior evoked by endothelin-1

[1]Departments of Anesthesiology, Psychiatry, and Developmental Biology, Washington University School of Medicine Pain Center, St. Louis, MO 63110, USA. [2]Department of Anesthesiology, Peking University Third Hospital, Beijing 100191, P.R. China.

*These authors contributed equally to this work.
†To whom correspondence should be addressed. E-mail: chenz@wustl.edu